A hybrid Boundary Element-Wave Based Method for the efficient solution of bounded acoustic problems with inclusions

Onur Atak[a,*], Stijn Jonckheere[a], Elke Deckers[a], Daan Huybrechs[b], Bert Pluymers[a], Wim Desmet[a]
[a]Department of Mechanical Engineering, KU Leuven, Celestijnenlaan 300b - Box 2420, B-3001 Leuven, Belgium
[b]Department of Computer Science, KU Leuven, Celestijnenlaan 200a, B-3001 Leuven, Belgium
email: onur.atak@mech.kuleuven.be, stijn.jonckheere@mech.kuleuven.be, elke.deckers@mech.kuleuven.be, daan.huybrechs@cs.kuleuven.be, bert.pluymers@mech.kuleuven.be, wim.desmet@mech.kuleuven.be

Abstract

This paper presents a novel hybrid approach for the efficient solution of bounded acoustic problems with arbitrarily shaped inclusions. The hybrid method couples the Wave Based Method (WBM) and the Boundary Element Method (BEM) in order to benefit from the prominent advantages of both. The WBM is based on an indirect Trefftz approach; as such, it uses exact solutions of the governing equations to approximate the field variables. It has a high computational advantage as compared to conventional element based methods, when applied on moderately complex geometries. The BEM, on the other hand, can tackle complex geometries with ease. However, it can be computationally expensive. The hybrid Boundary Element - Wave Based Method (BE-WBM) combines the best properties of the two; it makes use of the efficient WBM for the moderately complex bounded domains and utilizes the flexibility of the BEM for the complex objects that reside in the bounded domains. The accuracy and the efficiency of the method is demonstrated with three numerical examples, where the hybrid BE-WBM is shown to be more efficient than a quadratic Finite Element Method (FEM). While the hybrid method provides efficient solution for the bounded problems with inclusions, it also brings certain conceptual advantages over the FEM. The fact that it is a boundary-type method with an easy refinement concept reduces the modeling effort on the preprocessing step. Moreover, for certain optimization scenarios such as optimization of the position of inclusions, the FEM fails to provide a feasible solution because of its domain discretization requirements for each iteration. On the other hand, the hybrid method allows reusing of the fixed geometries and only needs recalculation of the coupling matrices without a further need of preprocessing. This makes its prominent efficiency even further emphasized.

Keywords: Wave Based Method; Boundary Element Method; Helmholtz Problem; Bounded Acoustic Problem; Inclusions; Trefftz Method.

1. Introduction

Numerical modeling techniques for steady-state acoustic problems have progressed over the years and became an integral part of engineering designs to reduce production costs. With the ever advancing technologies on the computing platforms, that role is becoming more and more pronounced. As the transition to virtual design is happening more strongly than ever, engineers are still in need of efficient methods. The ultimate goal of having one efficient method for all configurations and the full frequency range still seems far away. Therefore, efforts are spent on developing methods to remedy specific problems and frequency ranges. The focus of this paper is on low- and mid-frequency bounded acoustic problems.

For low-frequency bounded acoustic problems, the most established method is the Finite Element Method (FEM) [1]. Its ability to model complex geometries by fine discretization of the problem domain, together with the benefit of exploiting fast sparse solvers makes it a robust tool. However, as frequency increases, the

requirement for the refinement of the discretization results in very large systems, which are computationally expensive to solve. Moreover, using simple polynomial shape functions to describe the dynamic field variables, which are not the exact solutions of the governing equations, leads to pollution errors at higher frequencies [2, 3].

There have been various works on the improvement of the FEM, either from the optimization of the modeling process side [2, 4, 5] or by changing the underlying formulations [6, 7, 8, 9]. It is also possible to use iterative solvers and parallelization to speed up the solving process [10] and its combination with decomposition of the FEM domain [11].

While all these improvements and extensions add a great value to the FEM, the intrinsic properties of the method itself add certain difficulties on practical applications. The preprocessing step, which comprises the discretization of the domain and the refinement of the mesh for higher frequencies, adds costs to the whole modeling procedure. In addition, there can be an extra computational cost for bounded problems with inclusions, when the size of the mesh is driven by the details of the object and not by the frequency range of interest. Such geometrical configurations are common in engineering applications, especially with test setups, where the cavities have generally moderately complex geometries and the test subjects can have varying and detailed shapes. Various room acoustic applications have also similar settings. When certain optimization scenarios are considered for these geometries, e.g. where the shape and position of the inclusion is optimized, the use of the FEM can even be unfeasible because the domain has to be remeshed for each iteration.

Considering these issues, a novel hybrid method is proposed in this paper for the solution of bounded problems with complex inclusions. The Wave Based Method (WBM) [12, 13] and the Boundary Element Method (BEM) are coupled to provide an efficient solution to the problem and overcome the intrinsic conceptual problems of using the FEM. The philosophy of the hybrid Boundary Element-Wave Based Method (BE-WBM) is to benefit from the most prominent advantages of the coupled methods. The WBM is used to model moderately complex cavities and the BEM is used to model complex inclusions. By this way, the efficiency of the WBM is emphasized while the flexibility of the BEM widens the possible range of configurations that can be tackled.

The WBM belongs to the family of Trefftz methods [14, 12, 15, 16]. It has been applied to bounded and unbounded acoustic problems [13, 17], structural [18] and poroelastic problems [19] and combined vibro-acoustic problems [20, 21]. The main idea behind the WBM is to use *a priori* knowledge of the field to represent the main variables, in the form of function expansions that exactly satisfy the governing equation(s). One advantage of the WBM over the conventional FEM is that there is no extra pollution error (as defined in [2]) introduced on the field. The approximations are done through the boundary residuals, by enforcing them to zero with a Galerkin weighted residual formulation. Moreover, there is no need to go through a lengthy preprocessing stage, as the method is a meshless method and refinements can be done by simply increasing the number of wave functions. A sufficient condition for the WBM to converge is the convexity of the bounded domains or that the domain is decomposed into convex subdomains. However, for a good performance, a small number of large subdomains is preferred instead of a FEM like procedure of fine discretization. By this way, lengthy integrations on the interfaces are avoided and a general good conditioning of the system matrices is ensured. As such, the WBM shows its full efficiency for moderately complex geometries.

In the case of inclusion problems, even if the bounded domain itself is a moderately complex geometry, the convexity requirement is violated because of the presence of the inclusion, which then leads to further decomposition of the domain and the loss of efficiency. With the proposed hybrid method, it is possible to model the inclusion and the cavity as if they are two separate problems and couple them through a weighted residual formulation to build the system of equations. A direct solve algorithm is used afterwards. This approach avoids the decomposition of the large cavities, hence, increases the efficiency of the method. A similar philosophy was followed by the Multi-level WBM (ML-WBM), which is an extension to the conventional form of the method. With the ML-WBM, it is possible to isolate inclusions from the bounded domains, provided that they are coupled with unbounded wave functions. This requires the inclusion to be modeled within a circular truncation line for 2D problems or a spherical truncation surface for 3D problems. The inherent limitations of the WBM for complex geometries apply to the isolated inclusions of the ML-

WBM and drags the efficiency of the method for complex inclusions. In certain settings, such as the use of curved panels, it may not be feasible or possible to use the ML-WBM.

Another useful extension to the WBM, which aims to alleviate its limitations for complex geometries, is the hybrid Finite Element-Wave Based Method (FE-WBM) [22]. However, the method is aimed for cavities that have fine geometrical details on the boundaries rather than cavities with complex inclusions. In such a case, a thin layer of FEM elements can be used to model the outer parts of the geometry, while the WBM can be used to model the large acoustic cavity inside. Nevertheless, this approach runs into the same problems with the conventional WBM in the case of inclusion problems.

The hybrid BE-WBM for bounded domains follows the footsteps of the hybrid BE-WBM for multiple scattering problems [23]. However, instead of coupling the BEM with the unbounded wave functions, the BEM is coupled with bounded wave functions. This approach needs the definition of new coupling matrices as well as a new WBM submodel, which are presented in this paper. As such, the focus of this paper is on the derivation of the coupling algorithms, assessment of their accuracy and on the demonstration of the performance advantage of the hybrid method through numerical verifications. The method is derived and validated both for 2D and 3D problems.

As mentioned above, the hybrid method also aims to overcome the conceptual disadvantages of the FEM. One of the advantages of the hybrid method is the ease of pre-processing, in that, refinement of the model for higher frequencies only needs the discretization of the boundaries of the inclusions and increasing the number of wave functions. Another conceptual advantage of the proposed method is that, in the case of optimization problems where the topology or the position of inclusions/panels in large acoustic cavities are to be configured, the hybrid BE-WBM provides a very efficient solution. If the shape and position of the inclusions are to be optimized, the model for the cavity, i.e. the WBM submodel, can stay the same and only the BEM submodel and the coupling matrices need to be recalculated. If only the position needs to be changed, then only the coupling matrices need to be recalculated. Therefore, while the hybrid method provides a very efficient solution to forward problems, it also opens doors to efficient solving of inverse problems.

The paper is organized as follows: Section 2 gives the problem definition, Section 3 introduces the derivation of the hybrid BE-WBM and Section 4 demonstrates the efficiency and the accuracy of the method with 3 numerical examples. A discussion part at the end of Section 4 provides perspective to the presented results. Finally, the paper is concluded with a short summary and possible future topics in Section 5.

2. Problem Definition

The problem under consideration is a steady-state acoustic problem, where the acoustic pressure field $p(\vec{r})$ is governed by the inhomogeneous Helmholtz equation:

$$\nabla^2 p(\vec{r}) + k^2 p(\vec{r}) = -\mathrm{j}\,\rho_0 \omega \delta(\vec{r}, \vec{r}_q) q, \tag{1}$$

with k the acoustic wave number, δ the Dirac-delta function, ρ_0 the fluid density, ω the angular frequency and q a volume velocity source strength.

The problem boundary Γ can be divided in three non-overlapping parts based on the three types of commonly applied acoustic boundary conditions: $\Gamma = \Gamma_v \cup \Gamma_p \cup \Gamma_Z$. If one defines the velocity operator $\mathcal{L}_v(\bullet)$ as:

$$\mathcal{L}_v(\bullet) = \frac{\mathrm{j}}{\rho_0 \omega} \frac{\partial \bullet}{\partial n}, \tag{2}$$

where n is the normal vector, the boundary residuals can be written as:

$$\vec{r} \in \Gamma_v: \quad R_v(p(\vec{r})) = \quad \mathcal{L}_v(p(\vec{r})) - \overline{v}_n(\vec{r}) = 0, \tag{3}$$

$$\vec{r} \in \Gamma_p: \quad R_p(p(\vec{r})) = \quad p(\vec{r}) - \overline{p}(\vec{r}) = 0, \tag{4}$$

$$\vec{r} \in \Gamma_Z: \quad R_Z(p(\vec{r})) = \quad \mathcal{L}_v(p(\vec{r})) - \frac{p(\vec{r})}{\overline{Z}_n(\vec{r})} = 0. \tag{5}$$

The quantities $\overline{v}_n$, $\overline{p}$ and $\overline{Z}_n$ represent the imposed normal velocity, the imposed pressure and normal impedance, respectively.

The Helmholtz equation (1), together with the associated boundary conditions (3), (4) and (5) yields a fully defined mathematical formulation of the acoustic pressure field $p(\vec{r})$.

In order to avoid confusion on the upcoming hybrid BE-WBM formulas, the BEM boundaries are represented with S ,while the WBM boundaries are represented with Γ.

3. The hybrid Boundary Element - Wave Based Method for bounded problems with inclusions

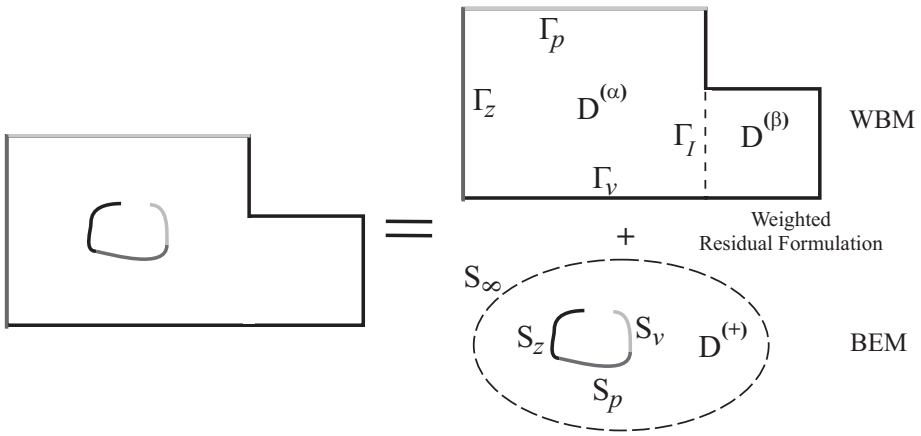

Figure 1: Graphic representation of the hybrid modeling concept, together with the sign conventions for subdomains and boundaries. The term $D^{(\bullet)}$ is used for the domains, $\Gamma_\bullet$ is for the WBM boundaries and interfaces and $S_\bullet$ is for the BEM boundaries.

The hybrid BE-WBM for bounded problems is built upon the superposition principle, in the same manner as it is for unbounded problems. The difference is that the field is decomposed into bounded and unbounded levels (see Figure 1), instead of being decomposed into only unbounded levels. The bounded part is assigned to the WBM, while the unbounded part can be a combination of the WBM and the BEM. In other words, the inclusions with simple geometries can still be modeled by using the unbounded WBM, following the principles of the ML-WBM [24]. However, the focus of this paper is on extending the WBM framework for geometrically complex inclusions. As such, the WBM submodel for modeling inclusions is omitted for the following formulas to have a better readability.

3.1. Domain decomposition

The concept for the decomposition of the domain into bounded and unbounded domains is illustrated in Figure 1. The bounded domain is associated with the WBM and the unbounded domain is associated with the BEM. In order to couple the two domains, one should first examine the decoupled problems on their own. The WBM pressure field is governed by:

$$\nabla^2 p_w^{(\alpha)}(\vec{r}_w) + k^2 p_w^{(\alpha)}(\vec{r}_w) = 0, \qquad \vec{r}_w \in D^{(\alpha)}, \tag{6}$$

where, $D^{(\alpha)}$ represents a bounded WBM domain. The BEM pressure field is governed by:

$$\nabla^2 p_b(\vec{r}_b) + k^2 p_b(\vec{r}_b) = 0, \qquad \vec{r}_b \in D^{(+)}, \tag{7}$$

with $D^{(+)}$ being an unbounded BEM domain. In addition, the BEM inherently satisfies the Sommerfeld radiation condition for 2D and 3D problems as follows:

$$\lim_{|\vec{r}_b|\to\infty} \left(|\vec{r}_b|^{\frac{n-1}{2}} \left(\frac{\partial p_b(\vec{r}_b)}{\partial |\vec{r}_b|} + jk p_b(\vec{r}_b) \right) \right) = 0, \quad \text{with: n = 2, 3.} \tag{8}$$

In their decoupled forms, $p_w^{(\alpha)}(\vec{r}_w)$ and $p_b(\vec{r}_b)$ are entirely determined by the conditions imposed on their own boundaries, $\Gamma_\bullet$ and $S_\bullet$. To retrieve the total pressure $p_{tot}^{(\alpha')}(\vec{r})$, where α' indicates combined fields, $p_w^{(\alpha)}(\vec{r}_w)$ and $p_b(\vec{r}_b)$ are coupled by matching $p_w^{(\alpha)}(\vec{r}_w) + p_b(\vec{r}_b)$ to $p_{tot}^{(\alpha')}(\vec{r})$ along the boundary $\{\Gamma_\bullet \cup S_\bullet\}$:

$$p_{tot}^{(\alpha')}(\vec{r}) = p_w^{(\alpha)}(\vec{r}) + p_b(\vec{r}), \qquad \vec{r} \in \{\Gamma_\bullet \cup S_\bullet\}. \tag{9}$$

In order for the above equation to hold for the combined domain, $D^{(\alpha')}$, the left hand side and the right hand side should solve the Helmholtz equation (1) in the field $D^{(\alpha')} = \left\{D^{(\alpha)} \cap D^{(+)}\right\}$. Indeed, this is the case, because the BEM satisfies the Sommerfeld radiation condition and the intersection of the BEM and the WBM domains results in the domain of interest. As such, equation (9) can be generalized to:

$$p_{tot}^{(\alpha')}(\vec{r}) = p_w^{(\alpha)}(\vec{r}) + p_b(\vec{r}), \qquad \vec{r} \in D^{(\alpha')}, \tag{10}$$

where $p_w^{(\alpha)}(\vec{r})$ is the pressure contribution from the WBM submodel, representing the bounded domain and $p_b(\vec{r})$ is the pressure contribution from the BEM submodel, representing the inclusion. Substituting this equation to the pressure definitions of both methods is the next step in deriving the hybrid BE-WBM system. The following two subsections detail the procedures for the WBM and the BEM submodels, respectively. For the remainder of the paper, the combined field pressure, $p_{tot}^{(\alpha')}(\vec{r})$, is written as $p_{tot}^{(\alpha)}(\vec{r})$ to have a better readability.

3.2. The WBM submodel

The Wave Based Method follows an indirect Trefftz approach [14], in that it uses expansions of functions that exactly satisfy the governing equation to represent the dynamic field variables. These functions are called wave functions. As such, the pressure contribution from the WBM submodel, $p_w^{(\alpha)}(\vec{r})$, is defined as follows:

$$p_w^{(\alpha)}(\vec{r}) \simeq \hat{p}_w^{(\alpha)}(\vec{r}) = \sum_{w=1}^{n_w^{(\alpha)}} \Phi_w^{(\alpha)}(\vec{r})\, t_w^{(\alpha)} + \hat{p}_f^{(\alpha)}(\vec{r}) = \Phi^{(\alpha)}(\vec{r})\, t^{(\alpha)} + \hat{p}_f^{(\alpha)}(\vec{r}), \qquad \vec{r} \in D^{(\alpha)}. \tag{11}$$

In this expression, α is the corresponding number of the bounded WBM subdomain. The functions $\Phi_w^{(\alpha)}$ represent *a priori* defined bounded wave functions and $t_w^{(\alpha)}$ are their corresponding contribution factors, $n_w^{(\alpha)}$ is the number of wave functions within subdomain $D^{(\alpha)}$. The term $\Phi^{(\alpha)}$ is the row vector collecting bounded wave functions and $t^{(\alpha)}$ is the column vector collecting weighting factors. Finally, $\hat{p}_f^{(\alpha)}$ represents a particular solution resulting from acoustic source terms q in the right hand side of the inhomogeneous Helmholtz equation (1). For the definition of 2D wave functions, the reader is referred to [12] and for the definition of 3D wave functions to [13]. The decision on the number of wave functions is made by using a truncation factor T. The suggested rule depends linearly on frequency. Wave functions that have wave number components smaller than or equal to the truncation factor T times the physical wave number k, are added to the wave function basis set. More details on this rule can be found in [13]. The truncation rule gives a better insight into the physical interpretation of the selection of wave functions. Typically a value between 1 to 4 is used for practical applications.

For the conventional WBM, it is equation (11) that is solely used to represent the field variable. For the hybrid method, the primary field variable definition is changed to equation (10).

For bounded problems, a sufficient condition for the WBM to converge is the convexity of the considered domain. For many practical applications, however, geometries are non-convex. Therefore, the acoustic domain has to be divided into convex subdomains. The main strategy in the decomposition process is to end up with a rather small number of large subdomains [12]. Following a FEM like approach and dividing the domain into very small parts causes the WBM to lose its efficiency. For this reason, the method is more suited for problems of moderate geometrical complexity.

To build up the system of equations for the WBM submodel, the boundary and interface conditions are enforced to zero through a weighted residual formulation. The interface conditions are needed to satisfy the

continuity among interfaces and couple acoustic subdomains. For the boundary residuals, equations (3), (4) and (5) are used. For the interface residuals, various coupling algorithms are available in the WBM literature [12]. The most common one is a direct equivalent normal velocity continuity condition and it is defined for the interface between two subdomains α and β as :

$$\vec{r} \in \Gamma_I : R_I^{(\alpha,\beta)} \left(p^{(\alpha)}(\vec{r}), p^{(\beta)}(\vec{r}) \right) = \left(\mathcal{L}_v(p^{(\alpha)}(\vec{r})) - \frac{p^{(\alpha)}(\vec{r})}{\overline{Z}_{int}} \right) + \left(\mathcal{L}_v(p^{(\beta)}(\vec{r})) + \frac{p^{(\beta)}(\vec{r})}{\overline{Z}_{int}} \right) = 0, \tag{12}$$

where $\overline{Z}_{int}$ is an impedance coupling factor which is chosen as the characteristic acoustic impedance $\rho_0\, c$ [12].

With boundary and interface conditions defined, the weighted residual formulation can be formed. For each subdomain, the residual functions are orthogonalized with respect to a weighting function $\tilde{t}^{(\alpha)}$ or its derivative. For N_D number of subdomains and $N_I^{(\alpha)}$ number of interfaces for each subdomain, it is written as :

$$\sum_{\alpha=1}^{N_D} \Big[\int_{\Gamma_v^{(\alpha)}} \tilde{t}^{(\alpha)}(\vec{r})\, R_v^{(\alpha)}(p_{tot}^{(\alpha)}(\vec{r}))\mathrm{d}\Gamma + \int_{\Gamma_Z^{(\alpha)}} \tilde{t}^{(\alpha)}(\vec{r})\, R_Z^{(\alpha)}(p_{tot}^{(\alpha)}(\vec{r}))\mathrm{d}\Gamma + \int_{\Gamma_p^{(\alpha)}} -\mathcal{L}_v^{(\alpha)}(\tilde{t}^{(\alpha)}(\vec{r}))\, R_p^{(\alpha)}(p_{tot}^{(\alpha)}(\vec{r}))\mathrm{d}\Gamma + \sum_{\beta=1,\beta\neq\alpha}^{N_I^{(\alpha)}} \int_{\Gamma_I^{(\alpha,\beta)}} \tilde{t}^{(\alpha)}(\vec{r})\, R_I^{(\alpha,\beta)} \left(p_{tot}^{(\alpha)}(\vec{r}), p_{tot}^{(\beta)}(\vec{r}) \right) \mathrm{d}\Gamma \Big] = 0, \tag{13}$$

where α and β are the corresponding subdomain numbers. It should be noted that the last term contains non-zero elements only for subdomains that have a common interface. Following a Galerkin approach, the weighting functions $\tilde{t}^{(\alpha)}$ are expanded in terms of the same set of acoustic wave functions used in the pressure expansion (11) :

$$\tilde{t}^{(\alpha)}(\vec{r}) = \sum_{w=1}^{n_w^{(\alpha)}} \Phi_w^{(\alpha)}(\vec{r}) t_w^{(\alpha)} = \Phi^{(\alpha)}(\vec{r})\, t^{(\alpha)}. \tag{14}$$

Substitution of the combined pressure definition (10) and the weighting function expansion (14) into the weighted residual formulation (13) yields the first part of the system of equations for the hybrid model.

3.3. The BEM submodel

For the BEM submodel, an indirect variational formulation is used. In its indirect form, the primary variables of the boundary integral equation are designated as the difference of the pressure, and the difference of the normal gradient of the pressure between both sides of the boundary surface [25] . These variables are named as double layer potential μ and single layer potential σ, respectively.

$$\mu(\vec{r}) = p(\vec{r}^{\,+}) - p(\vec{r}^{\,-}) \qquad \vec{r} \in S, \tag{15}$$

$$\sigma(\vec{r}) = \frac{\partial p(\vec{r}^{\,+})}{\partial n} - \frac{\partial p(\vec{r}^{\,-})}{\partial n} \qquad \vec{r} \in S. \tag{16}$$

By assuming a thin boundary, the single layer and double layer potentials are written for boundary conditions in equations (3), (4) and (5) as:

$$\mu(\vec{r}) = 0, \quad \vec{r} \in S_v \; ; \qquad \sigma(\vec{r}) = 0, \quad \vec{r} \in S_p \; ; \qquad \sigma(\vec{r}) = -jk\bar{\beta}\mu, \quad \vec{r} \in S_Z, \tag{17}$$

where $\bar{\beta} = \rho_0 c/\bar{Z}$. The pressure contribution $p_{\,b}(\vec{r})$ from the BEM submodel, which is given by the indirect boundary integral equations is written as :

$$\begin{aligned} p_{\,b}(\vec{r}) = &- \int_{S_p} \sigma(\vec{r}_a) G(\vec{r}, \vec{r}_a)\mathrm{d}S + \int_{S_v} \mu(\vec{r}_a) \frac{\partial G(\vec{r}, \vec{r}_a)}{\partial n(\vec{r}_a)}\mathrm{d}S \\ &+ \int_{S_Z} \mu(\vec{r}_a) \left(\frac{\partial G(\vec{r}, \vec{r}_a)}{\partial n(\vec{r}_a)} + jk\bar{\beta}(\vec{r}_a) G(\vec{r}, \vec{r}_a) \right) \mathrm{d}S, \end{aligned} \tag{18}$$

with $\vec{r}$ being the position vector where the field variable is calculated and $\vec{r}_a$ being the position vector on the boundary of the geometry. The reader is referred to [25] for the detailed information regarding the derivation of the indirect boundary integral equation. The Green's function $G(\bullet,\bullet)$ is defined for 2D problems as:

$$G(\vec{r},\vec{r}_a) = -\frac{j}{4}H_0^{(2)}(k\,|\vec{r}-\vec{r}_a|), \tag{19}$$

where $H_0^{(2)}$ is the zero-order Hankel function of the second kind and for 3D problems as:

$$G(\vec{r},\vec{r}_a) = \frac{e^{-jk|\vec{r}-\vec{r}_a|}}{4\pi\,|\vec{r}-\vec{r}_a|}. \tag{20}$$

A weighted residual formulation is applied on the boundary residuals to build up the BEM submodel.

$$\forall(\delta\sigma,\delta\mu): \qquad \int_{S_p} R_p(p_{tot}^{(\alpha)}(\vec{r}))\;\delta\sigma\;\mathrm{d}S + \int_{S_v} R_v(p_{tot}^{(\alpha)}(\vec{r}))\;\delta\mu\;\mathrm{d}S + \int_{S_Z} R_Z(p_{tot}^{(\alpha)}(\vec{r}))\;\delta\mu\;\mathrm{d}S = 0. \tag{21}$$

Following a Galerkin approach, the test functions are chosen the same as the potentials. Subsequently, substitution of the pressure definition (10) to above equation gives the BEM submodel of the hybrid system.

3.4. The hybrid system

Equations (13) and (21) should be solved together to get the unknowns of the hybrid system. The numerical discretization of the system leads to the following square matrix equation of n_{tot} number of degrees of freedom, where n_{tot} is the sum of degrees of freedom in the BEM submodel and the WBM submodel:

$$\begin{bmatrix} A_W & C_{WB} \\ C_{BW} & A_B \end{bmatrix} \begin{bmatrix} t \\ b \end{bmatrix} = \begin{bmatrix} F_W \\ F_B \end{bmatrix}. \tag{22}$$

where A_W is the system matrix of the WBM submodel and A_B of the BEM, as they would be in their standalone forms. C_{WB} and C_{BW} are the coupling matrices resulting from the extra pressure values in the boundary residuals coming from the companion method. F_W and F_B are the forcing terms coming from the prescribed variables of the corresponding methods. The terms t and b are the unknowns of the hybrid system, where t represents the unknown weighting factors of the corresponding wave functions and b represents the possible combination of the unknown potentials. After the system of equations is solved, the field pressure can be calculated by using the calculated wave function contribution factors and the potentials with equation (10).

A problem with Neumann boundary conditions is assumed to demonstrate what the system of equations looks like. In such a case, the system matrices and the right hand sides of the hybrid model are constructed as follows:

$$A_B = \int_{S_v}\int_{S_v} N_\mu(\vec{r}_a)\,N_\mu(\vec{r}_b)\,\frac{\partial G(\vec{r}_b,\vec{r}_a)}{\partial n(\vec{r}_a)\partial n(\vec{r}_b)}\mathrm{d}S\,\mathrm{d}S, \tag{23}$$

$$A_W = \int_{\Gamma_v} \frac{j}{\rho_0\omega}\Phi^T(\vec{r}_w)\;n^T(\vec{r}_w)\;B(\vec{r}_w)\,\mathrm{d}\Gamma, \tag{24}$$

$$C_{WB} = \int_{\Gamma_v} \frac{j}{\rho_0\omega}\Phi^T(\vec{r}_w)\int_{S_v} N_\mu(\vec{r}_a)\frac{\partial G(\vec{r}_a,\vec{r}_w)}{\partial n(\vec{r}_a)\partial n(\vec{r}_w)}\;\mathrm{d}S\,\mathrm{d}\Gamma, \tag{25}$$

$$C_{BW} = \int_{S_v} \Phi^T(\vec{r}_a)\,N_\mu(\vec{r}_a)\,\mathrm{d}S, \tag{26}$$

$$F_W = \int_{\Gamma_v} \Phi^T(\vec{r}_w)\;\bar{v}_n(\vec{r}_w)\;\mathrm{d}\Gamma, \tag{27}$$

$$F_B = \int_{S_v} j\rho_0\omega\bar{v}_n(\vec{r}_a)\;N_\mu(\vec{r}_a)\;\mathrm{d}S, \tag{28}$$

where $\vec{r}_a$ and $\vec{r}_b$ are the position vectors on the BEM boundaries and $\vec{r}_w$ is the position vector on the WBM boundaries. $N_\mu(\bullet)$ is the vector of global shape functions used in the discretization of the BEM boundaries. Finally, $B(\bullet)$ is the gradient of acoustic wave functions $\Phi(\bullet)$:

$$B(\bullet) = \nabla\Phi(\bullet). \tag{29}$$

The derivation of other boundary conditions and their combinations are straightforward and omitted here to avoid repetition.

4. Numerical verifications

In order to assess the accuracy and the performance of the method, three numerical verification cases are presented. The first verification case is a 2D problem, which aims to demonstrate the accuracy of the method and test the limits of the coupling algorithms. The second case is a 3D problem and is aimed at showing the convergence behavior of the method. The final case is also a 3D problem and demonstrates the performance of the method over a wide frequency range. Dirichlet, Neumann and Robin boundary conditions are used throughout different verifications. The reference methods for error calculations are chosen depending on the geometry of the verification case. For the first two cases, the BEM and the ML-WBM are used as references, while for the third case, the FEM is the reference. For all simulations, the acoustic medium is air with mass density, ρ_0, equal to 1.225 kg/m^3 and the speed of sound, c_0, equal to 340 m/s.

4.1. Accuracy assessment

The first case is chosen to effectively assess the accuracy of the coupling algorithms. The aim of this study is to indicate that the coupling algorithms do not introduce an extra error in the field and that the hybrid method manages to converge to the limit set by its least accurate submodel. In order to do so, full model references of the ML-WBM and the BEM are needed. As such, a simple geometry is chosen to provide a good ML-WBM reference.

A 2D problem is considered (see Figure 2) with a 1 m $\times$ 1 m square box and a circle with 0.25 m radius placed in the center of the box (with its origin at the coordinate (0,0)). Dirichlet boundary conditions are used for this case. The boundary of the box has a value of $\bar{p} = 1$ Pa and the boundary of the circle is assigned to $\bar{p} = 0$ Pa.

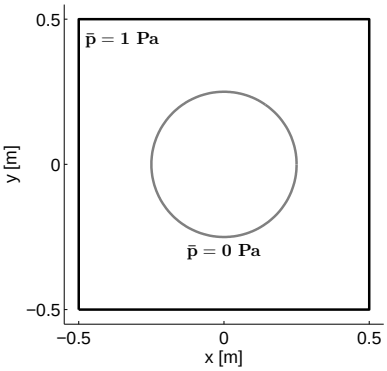

Figure 2: Problem geometry for the 2D case. The cavity boundaries are assigned to $\bar{p} = 1$ Pa and the circle boundary is assigned to $\bar{p} = 0$ Pa.

In order to assess the coupling accuracy, one part of the hybrid method (the WBM or the BEM submodel) is fixed and the other part is refined. Subsequently, the accuracy of the hybrid model is compared with the full BEM or full ML-WBM models that have the same degrees of freedom (DoF) on their associated

geometries, i.e. the circle for the BEM and the cavity for the ML-WBM. The simulations are run at 2000 Hz and 5000 Hz. The error criterion is chosen as the average of the relative error, which is defined as:

$$\epsilon_{av}(p(\vec{r})) = \frac{1}{N_{rp}} \sum_{i=1}^{N_{rp}} \frac{|p(\vec{r}_i) - p_{ref}(\vec{r}_i)|}{|p_{ref}(\vec{r}_i)|}, \tag{30}$$

where N_{rp} is the number of receiver points. For all the following convergence figures in this subsection, 60 post processing points are defined. The points are equally distributed on a circle of 0.35 m radius, whose origin is set at the coordinate (0,0). For the BEM reference, a Matlab [26] implementation of the method, which is based on [27], is used. The same code is used for the BEM submodel of the hybrid method.

Figures 3(a) and 3(b) show the case, where the number of DoF of the WBM submodel is fixed and the number of DoF of the BEM submodel is increased. The BEM submodel of the hybrid method uses linear elements with element lengths changing from 0.049 m to 0.001 m in 8 refinement steps. The reference model for the two figures is the ML-WBM. A high truncation rule of $T = 10$ is used to provide a good reference. The corresponding number of DoF of the reference model is given in the figures. The two straight lines with dashes and dots mark the accuracies given by the full ML-WBM models, when they use the same number of DoF on the box (with $T = 2$ and $T = 3$). It is clear that, when the hybrid method uses fixed WBM DoF, it converges to the limits given by the full ML-WBM models. When the number of DoF on the WBM submodel is chosen as equal to the reference ML-WBM model, the error curves keep converging. This shows that the coupling algorithms for the WBM submodel do not hinder the accuracy of the hybrid method.

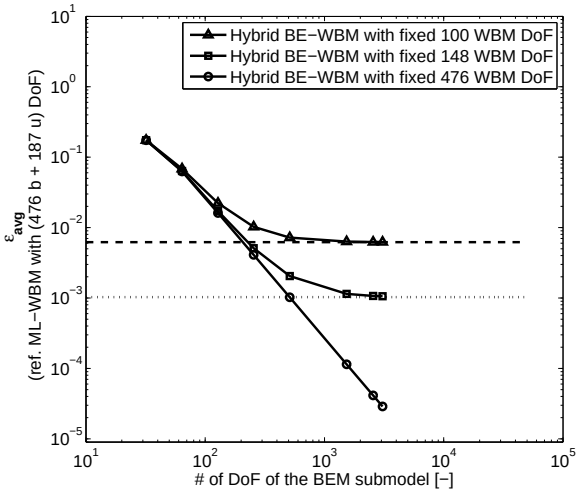

(a) 2000 Hz case. $(\cdots)$ represents the accuracy of the full ML-WBM model, which has 148 DoF for the cavity. (- -) represents the accuracy of the full ML-WBM model, which has 100 DoF for the cavity.

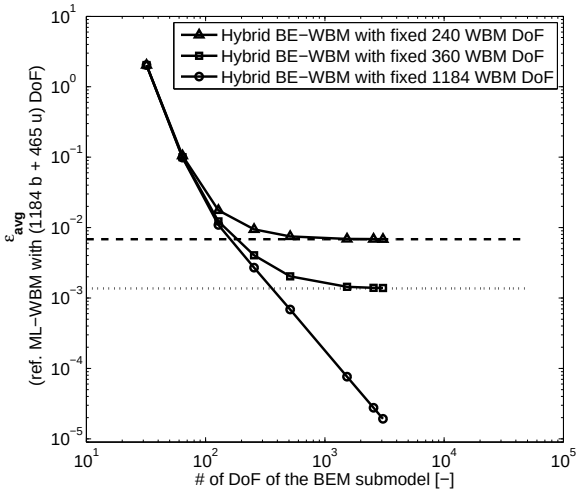

(b) 5000 Hz case. $(\cdots)$ represents the accuracy of the full ML-WBM model, which has 360 DoF for the cavity. (- -) represents the accuracy of the full ML-WBM model, which has 240 DoF for the cavity.

Figure 3: Convergence of the hybrid method with fixed DoF on the WBM submodel

Figures 4(a) and 4(b) show the case where the number of DoF of the BEM submodel is fixed and the number of DoF of the WBM submodel is increased. Each refinement corresponds to an integer value of truncation rule, with $T = 1 \ldots 10$. For this case, the reference is the BEM that uses linear elements. The two straight lines with dots and dashes show the limits of the BEM submodel. They are given by full BEM models that use the same element size (0.006 m and 0.003m) as the fixed submodel of the hybrid method. When the number of DoF of the WBM submodel is increased, the hybrid method converges to the limits for both cases of 2000 Hz and 5000 Hz. Moreover, when the BEM submodel of the hybrid BE-WBM is identical to that of the reference model's, the method keeps converging. These results demonstrate that the coupling algorithms for the BEM submodel also do not hinder the accuracy of the hybrid method.

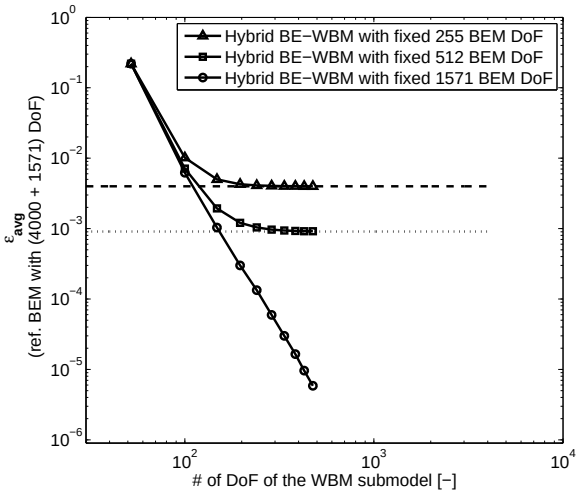

(a) 2000 Hz case. $(\cdots)$ represents the accuracy of the full BEM model, which has 512 DoF for the circle. (--) represents the accuracy of the full BEM model, which has 255 DoF for the circle.

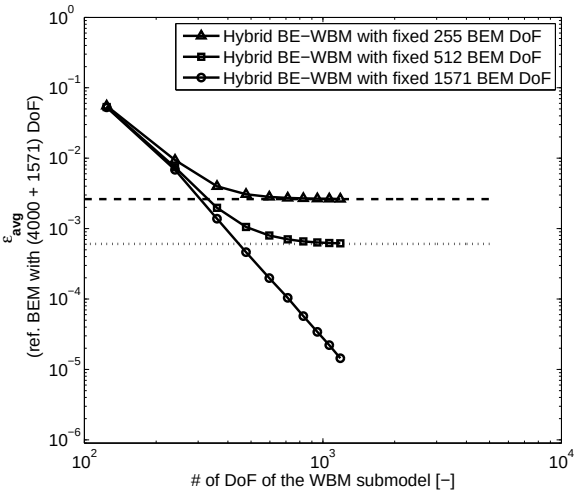

(b) 5000 Hz case. $(\cdots)$ represents the accuracy of the full BEM model, which has 512 DoF for the circle. (--) represents the accuracy of the full BEM model, which has 255 DoF for the circle.

Figure 4: Convergence of the hybrid method with fixed DoF on the BEM submodel

It is also of interest to examine the pressure field given by the hybrid BE-WBM and to see how it compares against a BEM reference. The same two frequencies are investigated: 2000 Hz and 5000 Hz. Figures 5 and 6 show the amplitude of the pressure at 2000 Hz for the BEM and the hybrid BE-WBM, respectively. Figure 7 shows the $\log_{10}$ of the relative error for the hybrid BE-WBM, defined as:

$$\epsilon(p(\vec{r})) = \frac{|p(\vec{r}) - p_{ref}(\vec{r})|}{|p_{ref}(\vec{r})|}, \tag{31}$$

where the reference is the BEM model. The BEM model uses element length of 0.001 m, which results in 4000 DoF for the cavity and 1571 DoF for the circle. The finest refinement model of the convergence figures is chosen for the hybrid method, which has 476 DoF ($T = 10$) for the WBM submodel (cavity) and 1571 DoF for the BEM submodel (circle).

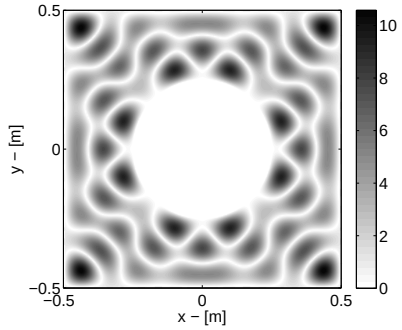

Figure 5: Pressure amplitude [Pa] at 2000 Hz given by the reference BEM.

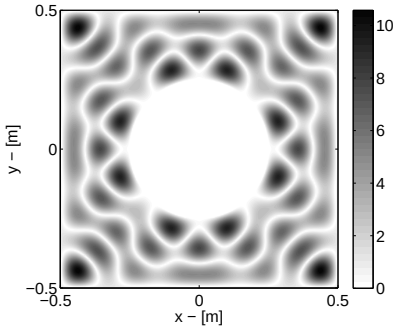

Figure 6: Pressure amplitude [Pa] at 2000 Hz given by the hybrid BE-WBM.

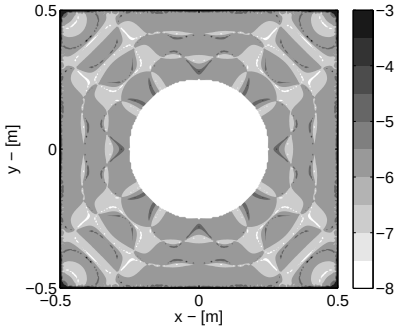

Figure 7: $\log_{10}(\epsilon)$ given by the hybrid BE-WBM (ref. BEM) at 2000 Hz.

Figures 8, 9 and 10 show the same quantities for 5000 Hz. The BEM model is kept the same. The hybrid method is again chosen as the finest refinement model on the convergence figures, which has 1184

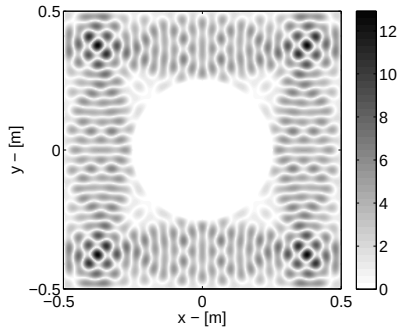

Figure 8: Pressure amplitude [Pa] at 5000 Hz given by the reference BEM.

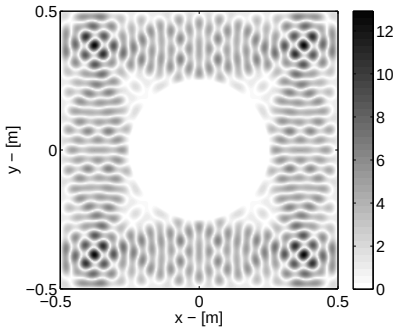

Figure 9: Pressure amplitude [Pa] at 5000 Hz given by the hybrid BE-WBM.

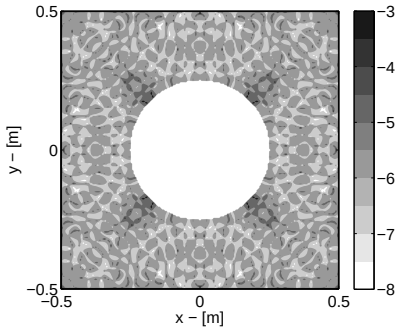

Figure 10: $\log_{10}(\epsilon)$ given by the hybrid BE-WBM (ref. BEM) at 5000 Hz.

DoF ($T = 10$) for the WBM submodel (cavity) and 1571 DoF for the BEM submodel (circle). As it is clearly seen on the figures, the hybrid method gives an excellent accuracy throughout the field.

With the given contour plots of the field and convergence figures, it is demonstrated that the coupling algorithms do not lower the accuracy of the hybrid BE-WBM and the method is driven by the accuracy of the least accurate of its submodels.

4.2. Performance assessment 1

The second verification case focuses on the convergence behavior of the method and how it compares to the FEM. The motivation is such that for bounded problems, the FEM is the state of the art and it is of interest to compare the convergence behaviors of the two methods. The problem geometry is given in Figure 11. The cavity is a 1 m × 1 m × 1 m cube. The inclusion is a sphere with 0.25 m radius, placed at the center of the cube at the coordinate (0,0,0). All the boundaries are rigid, i.e. $\bar{v}_n = 0$. The excitation to the system is a point source placed at the coordinate (0.3,0.3,0.3) with an amplitude of 1 m^3/s.

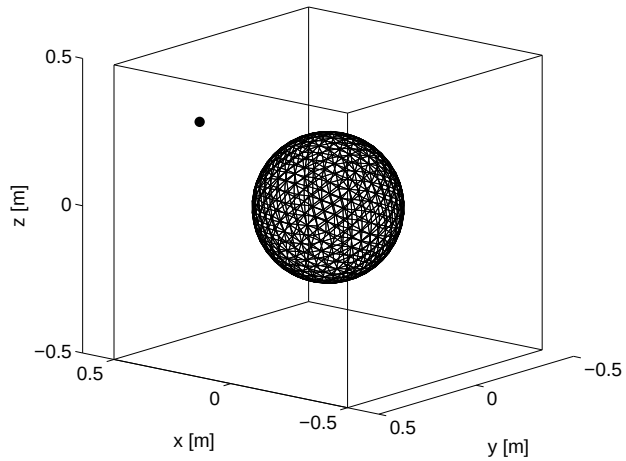

Figure 11: Problem geometry for the hybrid BE-WBM model. The point source (•) is located at the coordinate (0.3,0.3,0.3) and indicated with a black dot on the figure. All the boundaries are rigid ($\bar{v}_n = 0$)

It is of interest to see how the method behaves for successive refinements of the numerical models. As such, the performance of the method is evaluated with respect to its accuracy. The hybrid BE-WBM is compared to the conventional FEM for 500 Hz and 750 Hz in Figures 12 and 13. Two different element types are used for FEM models, i.e. linear tetrahedral elements and quadratic tetrahedral elements. The BEM submodel of the hybrid method uses linear triangular elements.

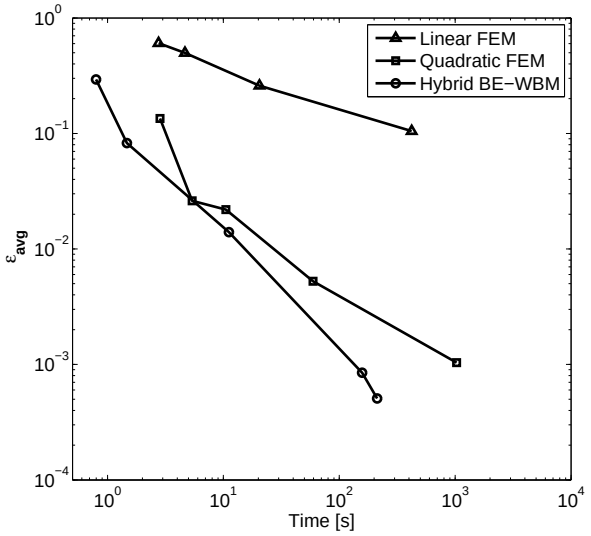

Figure 12: Convergence comparison of methods at 500 Hz (ref. ML-WBM with $T = 10$).

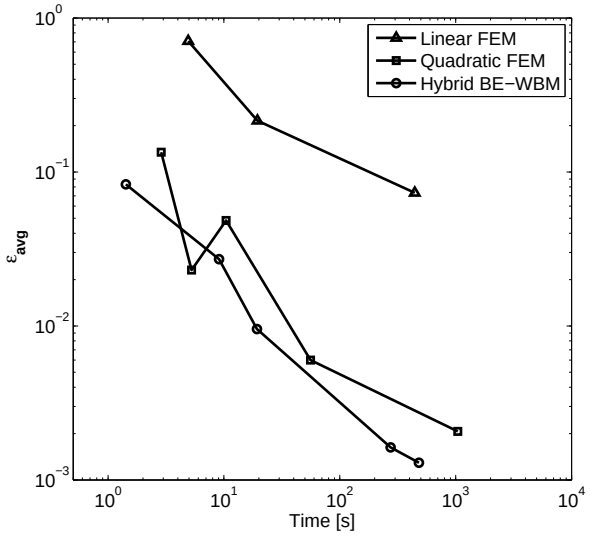

Figure 13: Convergence comparison of methods at 750 Hz (ref. ML-WBM with $T = 8$).

Equation (30) is used for the error criterion. The error is averaged over 42 points, which are equally distributed on a spherical surface with 0.4 m radius, placed in the center of the cavity at the coordinate (0,0,0). The corresponding numbers of DoF for the FEM and hybrid BE-WBM models are given in Tables 1 and 2 for 500 Hz and 750 Hz, respectively. The DoF of the hybrid method are obtained by combinations of $T = 1 \ldots 4$ for the WBM submodel and element sizes of 0.08 m, 0.04 m and 0.02 m for the BEM submodel. The reference model is the ML-WBM, which is very accurate and efficient for such a geometry [24]. For the 500 Hz case, the reference model has 5766 bounded and 625 unbounded wave functions, which corresponds to $T = 10$. For the 750 case, the reference model has 8214 bounded and 900 unbounded wave functions, which corresponds to $T = 8$.

Table 1: Model information for 500 Hz

	Number of DoF				
	refinement 1	refinement 2	refinement 3	refinement 4	refinement 5
Hybrid BE-WBM[a]	96 W + 162 B	294 W + 162 B	294 W + 642 B	600 W + 2562 B	1014 W + 2562 B
Quadratic FEM	6923	21762	42639	128679	506186
Linear FEM	5717	16845	65211	346350	-

[a] 'W' stand for the number of DoF of the WBM submodel and 'B' stands for the number of DoF of the BEM submodel.

Table 2: Model information for 750 Hz

	Number of DoF				
	refinement 1	refinement 2	refinement 3	refinement 4	refinement 5
Hybrid BE-WBM[a]	216 W + 162 B	216 W + 642 B	600 W + 642 B	1350 W + 2562 B	2166 W + 2562 B
Quadratic FEM	6923	21762	42639	128679	506186
Linear FEM	16845	65211	346350	-	-

[a] 'W' stand for the number of DoF of the WBM submodel and 'B' stands for the number of DoF of the BEM submodel.

The comparisons are made in terms of CPU times. For the hybrid method, the system matrices should be built for each frequency. As such, the CPU time is assigned as the sum of system building time and

system solving time. For the FEM, on the other hand, the system matrices are frequency independent. Consequently, only the system solving time is included in the CPU time. The benchmarks are run on a Linux machine with 8 Intel Xeon E5540, 2.53 GHz CPUs and 24 GB RAM. For all the models, one CPU is used to run the simulations, in order to make the comparison in a more controlled environment. However, effective parallelization is possible for both methods.

All the FEM models are calculated with Comsol 4.3 software [28]. The refinements of the FEM mesh are carried out by using the standard auto-meshing property of the software, such that the refinements follow the physical problem boundary and not the boundary of the previous mesh. The efficient MUMPS direct solver is used. For the hybrid method, an in-house research code is used, which is mainly based on Matlab [26]. A Fortran function is called from the Matlab to calculate the BEM submodel, which is created with inspiration from the sample codes in [25].

Figures 12 and 13 show clearly that the hybrid method has a better convergence behavior than the linear and quadratic FEM. The linear FEM struggles to get decent accuracy while having a heavy computational load. The quadratic FEM behaves better and shows good accuracy levels with reasonable computational time. However, when compared to the hybrid BE-WBM, it is roughly 5 times slower for its finest refinement models.

With the convergence figures presented, it is also of interest to see the error distribution on the field. Figure 14 shows the pressure field at 500 Hz predicted by the reference ML-WBM model. Figures 15 and 16 show $\log_{10}$ of the relative error (31) on the field given by the quadratic FEM and the hybrid BE-WBM, respectively. They are obtained by using the the finest refinements of both methods. The figures show the x-y plane at $z = 0$. Figures 17, 18 and 19 show the same quantities at 750 Hz.

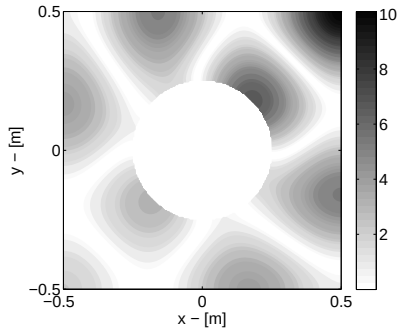

Figure 14: Pressure amplitude [Pa] at 500 Hz given by the ML-WBM with $T = 10$.

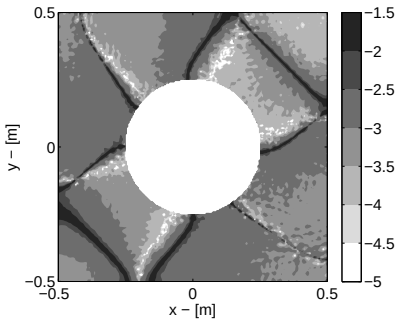

Figure 15: $\log_{10}(\epsilon)$ given by the quadratic FEM (ref. ML-WBM) at 500 Hz.

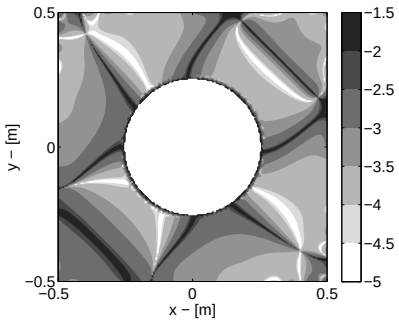

Figure 16: $\log_{10}(\epsilon)$ given by the hybrid BE-WBM (ref. ML-WBM) at 500 Hz.

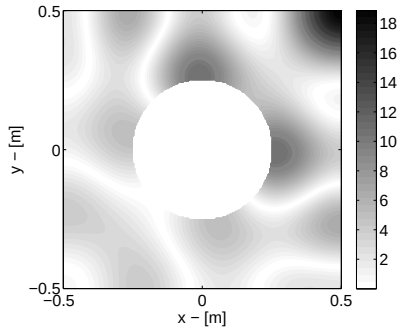

Figure 17: Pressure amplitude [Pa] at 750 Hz given by the ML-WBM with $T = 8$.

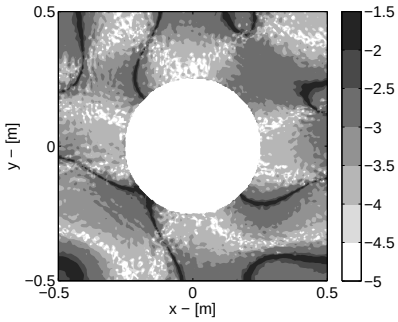

Figure 18: $\log_{10}(\epsilon)$ given by the quadratic FEM (ref. ML-WBM) at 750 Hz.

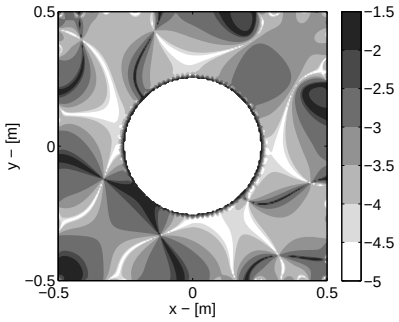

Figure 19: $\log_{10}(\epsilon)$ given by the hybrid BE-WBM (ref. ML-WBM) at 750 Hz.

The error distributions on the field confirms that a good overall accuracy is obtained for both methods. It is only at the lowest pressure zones that the accuracies drop to $10^{-1.5}$. This is the case for both the FEM and the hybrid BE-WBM and is due to the fact that the relative error calculation needs division of the error to the value of the reference pressure.

4.3. Performance assessment 2

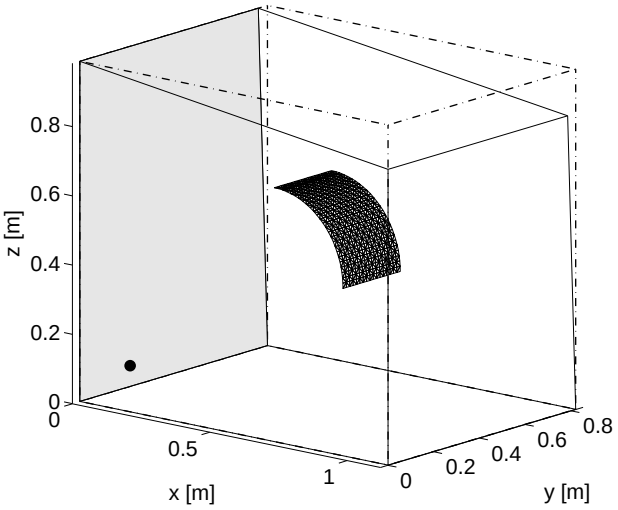

Figure 20: Problem geometry for the hybrid BE-WBM model. The point source (•) is located at the coordinate (0.1,0.1,0.1) and indicated with a black dot on the figure. All the boundaries are rigid ($\bar{v} = 0$), except the one at $x = 0$ coordinate, which is indicated by the gray color and has an impedance value of $\bar{Z}_n = 1000$ kg/m^{2}s

The third verification case aims to assess the performance of the hybrid BE-WBM over a wide frequency range and compares it to the FEM. The problem geometry is given in Figure 20. The cavity is a 1.122 m $\times$ 0.82 m $\times$ 0.982 m convex box with non-parallel walls. The inclusion is a zero-thickness curved panel, which is obtained by taking a quarter of a cylinder wall. The radius of curvature is 0.25 m and the length of the panel in y axis is 0.25 m. The center of the cylinder, which the panel is created from, is located at the coordinate (0.5,0.375,0.4). The geometry of the cavity is based on a test box at KU Leuven. More information can be found in [29, 30].

The problem geometry is chosen to demonstrate the flexibility of the hybrid BE-WBM. As such, this geometry is not feasible to model with a pure WBM or ML-WBM approach. The reason is that, decomposing the domain into convex subdomains would need a very fine discretization of the domain, which makes the WBM approaches inefficient.

All the boundaries of the problem are rigid ($\bar{v}_n = 0$), except the one at $x = 0$ coordinate, which is indicated by gray color on the figure and has an impedance value of $\bar{Z}_n = 1000$ kg/m^{2}s. The excitation is a point source placed at the coordinate (0.1,0.1,0.1), with an amplitude of 1 m^3/s.

Figure 21 shows the frequency response function(FRF) of the average pressure for three methods: hybrid BE-WBM, FEM with quadratic tetrahedral elements and an adaptive FEM with quadratic tetrahedral elements (as the reference). The pressure average is calculated over 42 equally distributed points on a spherical surface, with 0.4 m radius and its center located at the coordinate (0.6,0.4,0.5). The calculations are done from 100 Hz to 750 Hz, with 2.5 Hz steps.

In order to make a fair performance assessment, the accuracy of the models has to be identical. The model properties are adjusted for this purpose. The quadratic FEM model has 316037 nodes. The hybrid method has 486 DoF on the BEM submodel (element size is 0.015 m) and uses a truncation rule of $T = 3$ for the WBM submodel for all frequencies. As such, the number of DoF for the WBM submodel is between 54 and 1168 for the given frequency range. The adaptive quadratic FEM is chosen as the reference because

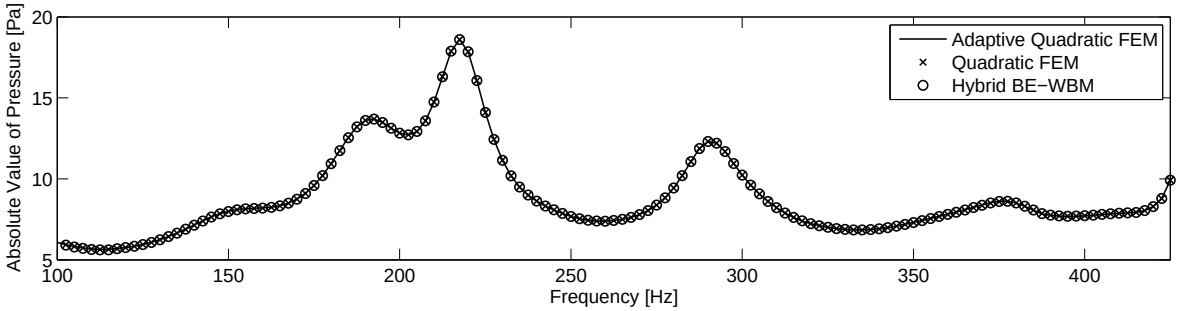

(a) Absolute value of pressure from 100 to 425 Hz

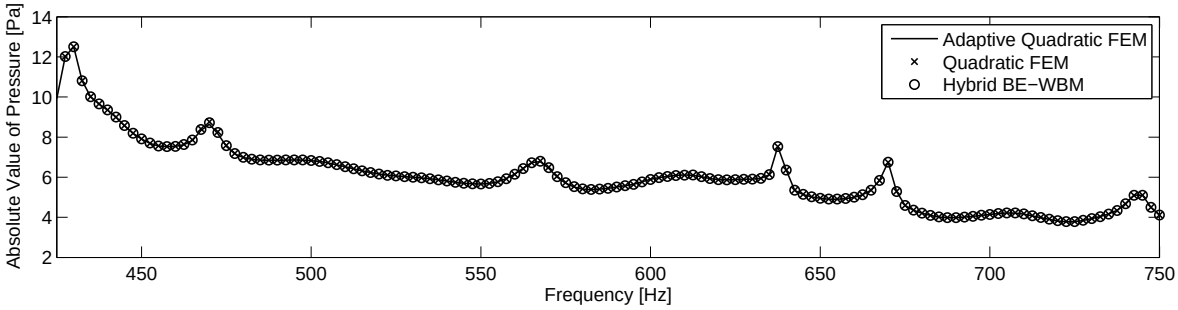

(b) Absolute value of pressure from 425 to 750 Hz

Figure 21: FRF comparison of methods. The frequency step is 2.5 Hz.

obtaining a quality reference model by a further refinement of the regular quadratic FEM model was not feasible due to heavy computational load and huge RAM requirement. The adaptive quadratic FEM uses a h-refinement strategy and is configured to have 20 successive refinements or a maximum number of 500000 elements. This results in an average of 964274 DoF over the whole frequency range. The FRF figure shows that all the methods nicely match with each other.

A more detailed look to the accuracy of the methods is given in Figure 22. The error is calculated for the same models and receiver points that are used to calculate the FRF curves. The relative error is calculated by using equation (30), with the adaptive quadratic FEM as the reference. It is apparent that the hybrid model and the quadratic FEM model have very similar accuracy, which is aimed to be around the engineering accuracy of 1 %.

It is also of interest to observe the error on the field. As such, Figure 23 shows the absolute value of the pressure at 500 Hz given by the adaptive quadratic FEM, while Figures 24 and 25 show the error field given by the quadratic FEM and the hybrid BE-WBM, respectively. Equation (31) is used to evaluate the error, while the adaptive quadratic FEM is chosen as the reference. The contours are given for x-z plane at $y = 0.4$. Figures 26, 27 and 28 present the same quantities at 750 Hz. The models used for the contour figures are the same models that are used to calculate the FRF curves. The hybrid method gives a slightly better accuracy as compared to the quadratic FEM for the presented frequencies, which is in agreement with Figure 22.

Overall, the accuracy of the two methods is adjusted to be very similar, which allows a fair comparison of performances. Figure 29 presents the cumulative CPU time over the given frequency range. The benchmarks are run using the same hardware and software with the previous verification case. Once again, the CPU time for the hybrid method includes system building and system solving time, while for the FEM, it corresponds to the system solving time. The total CPU time over the whole frequency range for the quadratic FEM is approximately 29 hours and for the hybrid BE-WBM, it is approximately 1.5 hours. As such, the hybrid method is almost 20 times faster than the quadratic FEM for this verification case.

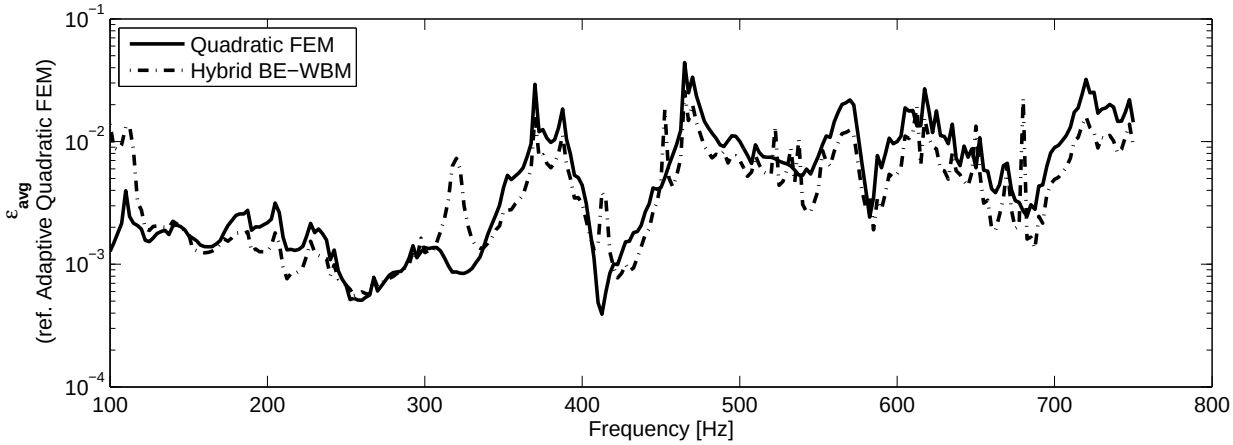

Figure 22: Comparison of relative error FRFs.

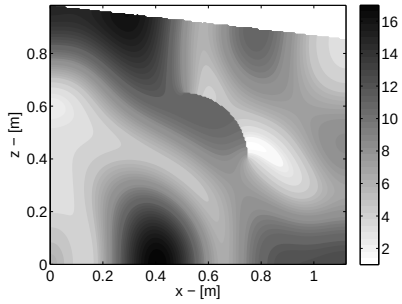

Figure 23: Pressure amplitude [Pa] at 500 Hz given by the adaptive quadratic FEM.

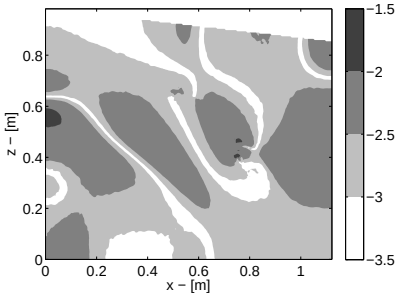

Figure 24: $\log_{10}(\epsilon)$ given by the quadratic FEM (ref. adaptive quadratic FEM) at 500 Hz.

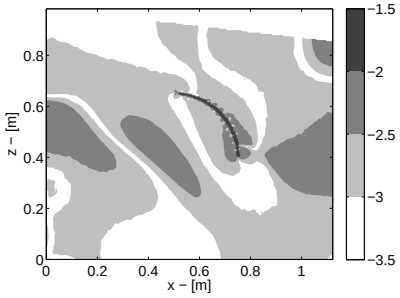

Figure 25: $\log_{10}(\epsilon)$ given by the hybrid BE-WBM (ref. adaptive quadratic FEM) at 500 Hz.

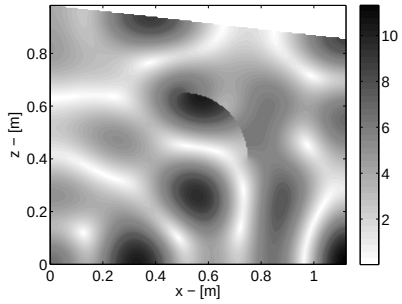

Figure 26: Pressure amplitude [Pa] at 750 Hz given by the adaptive quadratic FEM.

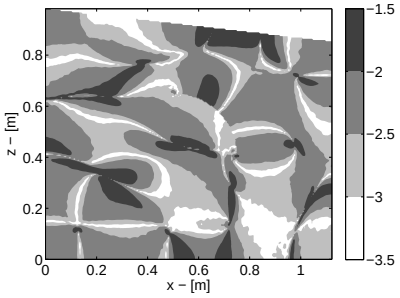

Figure 27: $\log_{10}(\epsilon)$ given by the quadratic FEM (ref. adaptive quadratic FEM) at 750 Hz.

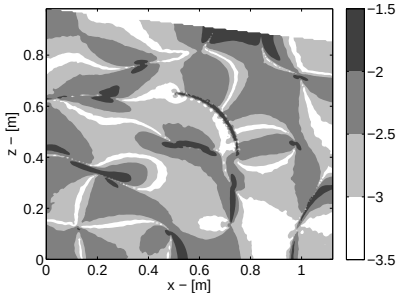

Figure 28: $\log_{10}(\epsilon)$ given by the hybrid BE-WBM (ref. adaptive quadratic FEM) at 750 Hz.

4.4. Discussion

It has been demonstrated that the hybrid BE-WBM gives high accuracy results while outperforming the FEM by almost 20 times for the last presented case.

Nevertheless, one should be cautious on interpreting the benchmark values presented in this section. The performance of the hybrid method depends on the relative size of the inclusion, as well as on the shape of the cavity. Having a very large inclusion would work in favor of the FEM, because the domain to be

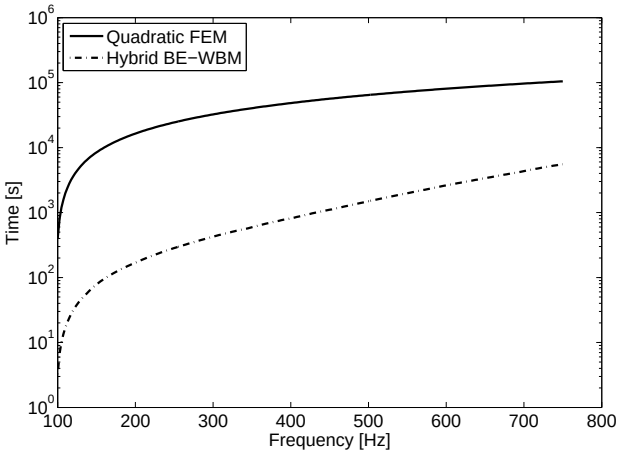

Figure 29: Comparison of cumulative CPU times.

modeled gets smaller, while for the hybrid method, it would cost an extra effort to model larger boundaries. Also, having a too complex cavity shape would drag the efficiency of the WBM submodel as well.

Beside the choice of the geometry, one should also note that the performance for both the FEM and the hybrid BE-WBM can be improved. The comparisons are made with an in-house code, mainly based on Matlab, for the hybrid BE-WBM and a commercial software, which uses an efficient implementation albeit a conventional version of the FEM. As such, improvements either from the methodological side (use of iterative solvers and accelerated schemes for the BEM and the FEM) or the implementation side is possible.

Keeping in mind all the above mentioned conditions, the authors believe that the performance figures presented here are indicative of the potential of the hybrid method and the cases are representative of possible engineering applications.

Moreover, the advantages of the hybrid method are not only about the raw performance figures, but also about the modeling concepts it uses. Namely, the ease of refinement of the models as compared to the FEM makes the pre-processing stage more user friendly and less time consuming. In addition, the possible use of the hybrid BE-WBM in an optimization scenario would make the already good performance figures even more pronounced. To be more specific, if the position of an inclusion is to be optimized with a fixed cavity, only the coupling matrices have to be recalculated for different iteration steps. If the shape of the inclusion is to be optimized, the WBM submodel can be reused. Considering that the system building time takes a considerable percentage of the total CPU time, this relaxation would bring an extra boost for the performance of the hybrid BE-WBM for both cases.

5. Conclusions

This paper proposes a novel hybrid method to efficiently solve bounded acoustic problems with inclusions. The WBM and the BEM are coupled to benefit from the best properties of the two. The WBM is used to model moderately complex cavities while the BEM is used to model complex inclusions. The use of indirect variational formulation for the BEM submodel allows the modeling of open boundary problems (zero thickness panels) and extends the possible range of applications. The method is derived for both 2D and 3D problems.

Three numerical verification cases are presented to assess the accuracy and the performance of the method. It has been demonstrated that the hybrid method is driven by the least accurate of its submodels and that the coupling algorithms do not hamper the accuracy. It has been also shown that the hybrid method exhibits a better convergence rate than the conventional FEM, for both linear and quadratic elements. Finally, a performance test over a wide frequency range shows that a hybrid BE-WBM model is almost 20 times faster than a quadratic FEM model.

Future work will focus on exploring the advantages of the hybrid method for optimization problems.

Acknowledgements

The authors kindly acknowledge the European Commission for supporting this research within the ENLIGHT Collaborative Research Project (GA 314567). Elke Deckers is a Postdoctoral Fellow of the Fund for Scientific Research - Flanders (F.W.O), Belgium. The research of Stijn Jonckheere is funded by a Ph.D. Grant of the Institute for the Promotion of Innovation through Science and Technology in Flanders (IWT-Vlaanderen).

References

[1] O. Zienkiewicz, R. Taylor, The Finite Element Method - The three volume set (6th ed.), Butterworth-Heinemann, 2005.
[2] P. Bouillard, F. Ihlenburg, Error estimation and adaptivity for the Finite Element Method in acoustics: 2D and 3D applications, Computer Methods in Applied Mechanics and Engineering 176 (1999) 147–163.
[3] S. Marburg, Six boundary elements per wavelength: is that enough?, Journal of Computational Acoustics 10 (2002) 25–51.
[4] I. Harari, D. Avraham, High-Order Finite Element Methods for Acoustic Problems, Journal of Computational Acoustics 05 (01) (1997) 33–51.
[5] W. Rachowicz, D. Pardo, L. Demkowicz, Fully automatic hp-adaptivity in three dimensions, Computer Methods in Applied Mechanics and Engineering 195 (3740) (2006) 4816–4842.
[6] I. Babuška, S. Sauter, Is the Pollution Effect of the FEM Avoidable for the Helmholtz Equation Considering High Wave Numbers?, SIAM Review 42 (3) (2000) 451–484.
[7] O. Cessenat, B. Desprs, Using Plane Waves as Base Functions for Solving Time Harmonic Equations with the Ultra Weak Variational Formulation, Journal of Computational Acoustics 11 (02) (2003) 227–238.
[8] C. Farhat, I. Harari, L. P. Franca, The discontinuous enrichment method, Computer Methods in Applied Mechanics and Engineering 190 (48) (2001) 6455–6479.
[9] C. Farhat, I. Harari, U. Hetmaniuk, A discontinuous Galerkin method with Lagrange multipliers for the solution of Helmholtz problems in the mid-frequency regime , Computer Methods in Applied Mechanics and Engineering 192 (1112) (2003) 1389–1419.
[10] Y. Erlangga, Advances in iterative methods and preconditioners for the helmholtz equation, Archives of Computational Methods in Engineering 15 (1) (2008) 37–66.
[11] C. Farhat, A. Macedo, M. Lesoinne, F.-X. Roux, F. Magouls, A. de La Bourdonnaie, Two-level domain decomposition methods with Lagrange multipliers for the fast iterative solution of acoustic scattering problems, Computer Methods in Applied Mechanics and Engineering 184 (24) (2000) 213–239.
[12] B. Pluymers, B. Van Hal, D. Vandepitte, W. Desmet, Trefftz-based methods for time-harmonic acoustics, Archives of Computational Methods in Engineering 14 (2007) 343–381.
[13] B. Van Genechten, O. Atak, B. Bergen, E. Deckers, S. Jonckheere, J. Lee, A. Maressa, K. Vergote, B. Pluymers, D. Vandepitte, W. Desmet, An efficient wave based method for solving helmholtz problems in three-dimensional bounded domains, Engineering Analysis with Boundary Elements 36 (1) (2012) 63–75.
[14] E. Trefftz, Ein Gegenstück zum Ritzschen Verfahren, in: Second International Congress on Applied Mechanics, Zurich, Switserland, 1926, pp. 131–137.
[15] G. Fairweather, P. M. A. Karageorghis, The method of fundamental solutions for scattering and radiation problems, Engineering Analysis with Boundary Elements 27 (2003) 759–769.
[16] G. H. Koopmann, L. Song, J. B. Fahnline, A method for computing acoustic fields based on the principle of wave superposition, Journal of Acoustic Society of America 86 (1989) 2433–2438.
[17] B. Bergen, B. Pluymers, B. Van Genechten, D. Vandepitte, W. Desmet, A trefftz based method for solving helmholtz problems in semi-infinite domains, Engineering Analysis with Boundary Elements 36 (1) (2012) 30–38.
[18] K. Vergote, C. Vanmaele, D. Vandepitte, W. Desmet, An efficient wave based approach for the time-harmonic vibration analysis of 3D plate assemblies , Journal of Sound and Vibration 332 (8) (2013) 1930–1946.
[19] E. Deckers, N.-E. Hörlin, D. Vandepitte, W. Desmet, A wave based method for the efficient solution of the 2d poroelastic biot equations, Computer Methods in Applied Mechanics and Engineering 201-204 (2012) 245–262.
[20] B. Van Genechten, D. Vandepitte, W. Desmet, A direct hybrid Finite Element - Wave Based modelling technique for efficient coupled vibro-acoustic analysis, Computer Methods in Applied Mechanics and Engineering 200 (5-8) (2011) 742–764.
[21] S. Jonckheere, E. Deckers, B. V. Genechten, D. Vandepitte, W. Desmet, A direct hybrid Finite Element Wave Based Method for the steady-state analysis of acoustic cavities with poro-elastic damping layers using the coupled Helmholtz-Biot equations, Computer Methods in Applied Mechanics and Engineering 263 (0) (2013) 144–157.
[22] B. Van Genechten, B. Pluymers, D. Vandepitte, W. Desmet, A Hybrid Wave Based - Modally Reduced Finite Element Method for the Efficient Analysis of Low- and Mid-frequency Car Cavity Acoustics, SAE International Journal of Passenger Cars - Mechanical Systems 2 (1) (2009) 1494–1504.

[23] O. Atak, B. Bergen, D. Huybrechs, B. Pluymers, W. Desmet, Coupling of boundary element and wave based methods for efficient solving of complex acoustic multiple scattering problems, Accepted for publication in Journal of Computational Physics.
[24] B. Van Genechten, K. Vergote, D. Vandepitte, W. Desmet, A Multi-Level Wave Based numerical modelling framework for the steady-state dynamic analysis of bounded Helmholtz problems with multiple inclusions, Computer Methods in Applied Mechanics and Engineering 199 (29-32) (2010) 1881–1905.
[25] T. Wu, Boundary Element Acoustics, Fundamentals and Computer Codes, WIT Press, 2000.
[26] MATLAB, version 7.10.0 (R2010a), The MathWorks Inc., Natick, Massachusetts, 2010.
[27] D. Huybrechs, S. Vandewalle, An efficient implementation of boundary element methods for computationally expansive green's functions, Engineering Analysis with Boundary Elements 32 (2008) 621–632.
[28] Comsol Multiphysics, version 4.3, Comsol, Inc., 2012.
[29] M. Vivolo, S. Jonckheere, B. Pluymers, D. Vandepitte, W. Desmet, Broadband sound absorption measurements by means of a small cabin, submitted to Journal of the Acoustical Society of America.
[30] M. Vivolo, B. Pluymers, B. Van Genechten, D. Vandepitte, W. Desmet, Study of the vibro-acoustic behaviour of composite sandwich structures by means of a novel test setup, in: International Conference on Noise and Vibration Engineering (ISMA2012), Leuven, Belgium, September 2012.